Journal Pre-proof

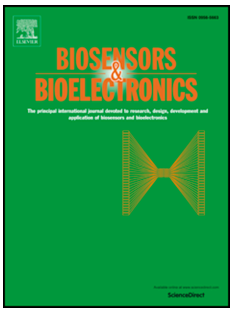

A novel signal amplification strategy based on the competitive reaction between 2D Cu-TCPP(Fe) and polyethyleneimine (PEI) in the application of an enzyme-free and ultrasensitive electrochemical immunosensor for sulfonamide detection

Jiaxuan Xiao, Xialin Hu, Kun Wang, Yanmin Zou, Eric Gyimah, Salome Yakubu, Zhen Zhang

PII: S0956-5663(19)30962-5

DOI: https://doi.org/10.1016/j.bios.2019.111883

Reference: BIOS 111883

To appear in: *Biosensors and Bioelectronics*

Received Date: 16 August 2019

Revised Date: 27 October 2019

Accepted Date: 12 November 2019

Please cite this article as: Xiao, J., Hu, X., Wang, K., Zou, Y., Gyimah, E., Yakubu, S., Zhang, Z., A novel signal amplification strategy based on the competitive reaction between 2D Cu-TCPP(Fe) and polyethyleneimine (PEI) in the application of an enzyme-free and ultrasensitive electrochemical immunosensor for sulfonamide detection, *Biosensors and Bioelectronics* (2019), doi: https://doi.org/10.1016/j.bios.2019.111883.

Revision submitted to ***Biosens. Bioelectron.***

MS Ref No. BIOS-D-19-02660

A novel signal amplification strategy based on the competitive reaction between 2D Cu-TCPP(Fe) and polyethyleneimine (PEI) in the application of an enzyme-free and ultrasensitive electrochemical immunosensor for sulfonamide detection

Jiaxuan Xiao[1], *Xialin Hu*[2*], *Kun Wang*[3], *Yanmin Zou*[4], *Eric Gyimah*[1], *Salome Yakubu*[1], *Zhen Zhang*[1*]

[1]School of the Environment and Safety Engineering, Jiangsu University, Zhenjiang 212013, China

[2]Key Laboratory of Yangtze River Water Environment, Ministry of Education, College of Environmental Science and Engineering, Tongji University, 1239 Siping Road, Shanghai, 200092, China

[3]The School of Chemistry and Chemical Engineering, Jiangsu University, Zhenjiang 212013, China

[4]School of Pharmacy, Jiangsu University, Zhenjiang 212013, China

* Corresponding author:

E-mail: xialin.hu@gmail.com; zhangzhen@ujs.edu.cn

Fax: +86-511-88790955

ABSTRACT

Nanozymes with peroxidase-like activity have been widely used as signal labels in electrochemical immunosensors. However, these sensors always suffer from some shortcomings during the processes underlying nanozyme labeling, including complex reactions, nanozyme inactivation after being decorated on the antibodies. To solve these problems, a novel electrochemical immunosensor was designed for ultrasensitive detection of sulfonamides (SAs), in which the synthesized 2D Cu-TCPP(Fe) with peroxidase-like property was used as a nanozyme that was directly modified on the electrode surface. Meanwhile, the structure of 2D Cu-TCPP(Fe) could be destroyed by the polyethyleneimine (PEI) from PEI-GO@Ab_2 due to the stronger affinity between PEI and Cu^{2+}, leading to an activity change of the prepared nanozyme. When H_2O_2 was introduced to the system, the electrochemical current was significantly declined owing to the peroxidase activity of 2D Cu-TCPP(Fe) decreased, which led to signal amplifications. Under the optimized conditions, this strategy had a wide detection range (1.186-28.051 ng/mL), satisfactory accuracy and precision (recoveries, 64-118%; CV, 2.16- 7.27%) with a low detection limit of 0.395 ng/mL. The findings of this study indicate that the electrochemical immunosensor we developed has great potential and can be used for enzyme-free detection of SAs in environmental samples.

Keywords:

Immunoassay, signal amplification, electrochemical biosensor, nanozyme, sulfonamides

1. Introduction

Sulfonamides (SAs), a generic class of broad-spectrum antibiotics with the structure of p-aminobenzene sulfonamide(Ma et al. 2016; Managaki et al. 2007), have been widely used as prophylactic agents/medicines for treating diseases in humans and as growth additives in domestic animals depending on their good stability and low cost(Dinh et al. 2017). Extensive use of SAs brings about their ubiquitous occurrence in aquatic environments via excreted feces and urine, contributing to the evolution of antibiotic resistant genes and damaging public health(Lu et al. 2015). Accordingly, there are increasing concerns about the direct or indirect impact of SA residues on aquatic ecosystems and the resulting antibiotic resistant genes(Kim et al. 2013; Lu et al. 2015). Hence, it is necessary to establish an effective method to investigate SAs in environmental waters for risk assessments.

At present, various analytical methods have been reported for SAs analysis, including gas chromatography-mass spectrometry (GC-MS)(Loos et al. 2017), high performance liquid chromatography(Du et al. 2017; Jia et al. 2018), high-performance liquid chromatography coupled with triple quadrupole mass spectrometry (HPLC–MS/MS)(Nebot et al. 2013; Won et al. 2011) and capillary electrophoresis(Hernández-Mesa et al. 2019; Shuo et al. 2018). Although these approaches have shown some advantages, including good sensitivity and accurate quantification, their drawbacks (e.g., tedious sample pretreatment procedures, the requirement of large amounts of organic solvents for enrichment and cleanup, and expensive instruments) have hindered their further application(Liu et al. 2016; Luo et al. 2010; Shoeib et al. 2004). By comparison, electrochemical immunoassays displayed some obvious advantages for SA determination because of their low cost, high accuracy, portability and simplicity(Conzuelo et al. 2013; Conzuelo et al. 2012). However, the performance of immunoassays using natural enzymes would be potentially influenced by the extremely complex environmental conditions, resulting in irreversible deformation. To address the issue, nanozyme-based electrochemical immunoassays were introduced into the detection system.

Nanozymes have been defined as a kind of nanomaterial with intrinsic enzymatic activities(Gao et al. 2007; Shan et al. 2007), including metal oxides, metal sulfide and metal-organic frameworks (MOFs), which have attracted considerable attention in many fields because of their low cost, high stability and good tolerance against different matrixes(Dong et al. 2019; Zhou et al. 2017; Zhu et al. 2019). However, despite their indispensable advantages, the potential drawbacks of some conventional nanozymes have limited their further application, such as the fact that only a small number of active sites were exposed on the surface of materials and the bio-recognition sites of nanozymes were hindered by their small surface-to-volume ratio(Zhang et al. 2019; Zhou et al. 2017). To overcome the aforementioned limitations, nanozymes based on a two-dimensional (2D) structure were designed and exhibited excellent catalytic properties(Walper et al. 2018; Zhu et al. 2018). The 2D metal-organic frameworks (MOFs) showed distinct merits owing to their large surface area and lower diffusion barriers, which were conducive to simpler substrate molecules being exposed on the surface of active sites(Chen et al. 2018). Cheng et al. established an attractive bioassay to monitor the Hep elimination process in live rats with 2D Zn-TCPP(Fe), which displayed high activity for mimicking peroxidase(Cheng et al. 2017). By means of AuNPs grown on 2D MOFs, Huang et al. designed an interesting strategy to mimic natural enzymes and catalyze cascade reactions(Huang et al. 2017). In addition, Liu et.al developed a strategy to decrease the pH of wounds and achieved a significant antibacterial effect via 2D Cu-TCPP(Fe) *in vivo*(Liu et al. 2019b).

Inspired by the above-mentioned literatures, at the present study, a novel electrochemical immunosensor strategy was designed for ultrasensitive determination of SAs in aquatic environments, in which 2D MOFs with peroxidase properties were directly decorated on the surface of electrodes (shown as **Scheme 1)**. This strategy showed obvious merits on preventing the loss of catalytic activity during nanozyme labeling. After evaluating its performance (accuracy, precision and stability), the proposed immunosensor was applied for real environmental sample analysis.

2. Experimental section

Materials, reagents, apparatus, electrochemical parameter and sample preparation were displayed in **S1-4**.

2.1. Synthesis of 2D Cu-TCPP(Fe) nanosheets

2D Cu-TCPP(Fe) nanosheets were synthesized according to a previous report with minor modifications(Qin et al. 2018b). $Cu(NO_3)_2 \cdot 3H_2O$ (7.2 mg, 0.015 mM), trifluoroacetic acid (20 μL, 1.0 M), and PVP (20.0 mg) were dissolved in DMF-ethanol (Volume ratio=3:1, 24 mL), and then, TCPP (Fe) (8.0 mg, 0.005 mM) dissolved in a DMF-ethanol mixture (volume ratio = 3:1, 8 mL) was added dropwise into 24 mL of the prepared solution under vigorous stirring. After 10 min of ultrasound, the resulting mixture was heated for 18 h at 80 °C. The final solution was cooled and centrifuged, and the resulting sediment was washed several times with ethanol. The obtained 2D nanosheets were re-dispersed in ultrapure water.

2.2. Synthesis of PEI-GO@Ab_2

To increase water solubility, carboxyl-functionalized GO (GO-COOH) was synthesized according to previous reports(Jing et al. 2017). Under stirring, 200 mg GO in HNO_3-H_2SO_4 (Volume ratio = 1:3, 40 mL) was refluxed for 8 h at 60 □. After filtration through 0.22 μm filters, GO-COOH was dried under vacuum. Finally, the product was stored at 4 °C until use.

Ten milligrams GO-COOH and 100 mg PEI were dissolved in 20 mL ultrapure water under 30 min of ultrasound. Then, 200 mg EDC was added to the mixture. After 8 h of stirring, the PEI-GO suspension was centrifuged and then dried under vacuum. For the preparation of PEI-GO@Ab_2, 1 mL Ab_2 (10 μg/mL) was mixed with the 3 mL PEI-GO (6 mg/mL) suspension at 4 °C. After 12 h of stirring, 100 μL of 1% BSA was used to block non-specific sites. The collected PEI-GO@Ab_2 was redissolved in PBS (0.01 mol/L, pH= 7.4) and stored at 4 °C.

2.3. Electrode modification.

The bare GCEs were repeatedly polished both 0.3 μm alumina slurries. Then, the GCEs were ultrasonically washed in ultrapure water and dried under nitrogen.

Subsequently, 6 μL MWCNTs (3 mg/mL) were modified on the surface of GCEs. After drying at 25□, 6 μL Cu-MOFs (6 mg/mL) were coated onto the modified electrode surface.

2.4. Fabrication of the electrochemical immunosensors

Six microliters of the antigen was modified on the electrode surface overnight at 4 □. To prevent nonspecific binding, after washing, the surface of the electrode was blocked with BSA and incubated at 37 □ for 45 min. After washing once, 3 μL of Ab_1 and the same volume of sample (or standard Sulfamonomethoxine, abbreviated to SMM)) were sequentially decorated on the electrode surface. After incubation and washing, 6 μL PEI-GO@Ab_2 was dropped onto the surface of the modified GCEs. After reacting at 37 °C for 40 min and washing again, the electrode was submerged in PBS containing 10 mM H_2O_2.

3. Results and discussion

3.1. Characterization of MWCNTs, Cu-TCPP(Fe) and PEI-GO

The morphology of MWCNTs was characterized by TEM. As displayed in **Fig. S2**, the MWCNTs indicated remarkable tubular structure and without any impurities on their surface.

TEM and SEM images of Cu-TCPP(Fe) showed obvious crumpled and curled planes (**Fig. 1A and 1B**), which were caused by the dimensional characteristics of the 2D structure, indicating that the material was successfully synthesized. Additionally, SEM element mapping indicated that the C, N, O, Fe, and Cu in the nanosheet were homogeneously distributed (**Fig. 1C**).

The morphology of GO and PEI-GO were characterized via TEM and SEM images, respectively. As shown in **Fig. 2A and 2B**, GO indicated clear wrinkling with a sheet morphology. By contrast, the wrinkling of PEI-GO was blurred and unable to be clearly observed (**Fig. 2C and 2D**) because PEI was modified on the surface of GO. The result was further confirmed by FT-IR and zeta potential measurement. As displayed in Fig. 3, GO presented peaks at 3428, 1731, and 1624 cm^{-1} associated with −OH, C=O, and the C=C stretching vibration (curve a), respectively, consistent with

the previous literature(Huang and Bo 2018). By comparison, a peak (2918 cm^{-1}, as observed in curve b) appeared at the FT-IR of PEI-GO, corresponding to the stretching vibration of $–CH_2$ at the PEI chain. Moreover, PEI-GO showed a new vibration band at approximately 1630 cm^{-1}, matching N-C=O and suggesting that PEI had been modified on the surface of GO. Meanwhile, zeta potential measurement (Fig. S3) indicated that the zeta potential value of GO was – 15.1 mV. After modification with PEI, the value of zeta potential was dramatically changed to + 41.0 mV, which could be caused by the high density amino-groups with positive charges was attributed on the surface of PEI-GO, confirming that the successful surface modification of GO with the PEI.

3.2. Mechanism of the Electrochemical Immunosensor

Scheme 1 depicts the protocol for this competitive electrochemical immunosensor, which applied 2D Cu-TCPP(Fe) as a novel nanozyme for signal amplifications.

In addition, Cu-TCPP(Fe) was demonstrated with the peroxidase-mimicking activities(Cheng et al. 2017; Qin et al. 2018a), and the current response of Cu-TCPP(Fe) was mainly caused by TCPP(Fe) as dominant active sites that could be reacted with H_2O_2. Moreover, Cu^{2+} acted as the junction sites could enhance the structural stability of 2D MOFs. After Cu-TCPP(Fe) bonded with the PEI-GO, the signal of 2D MOFs was remarkably decreased, which was probably due to that the Cu-TCPP(Fe) could be collapsed by PEI and released the TCPP(Fe) inside. At the same time, PEI was a good chelating agent that could bond with Cu (II), resulting in TCPP(Fe) being released (Zhang et al. 2016). Actually, GO possess the ability to adsorb Cu^{2+}, however, the adsorption capacity of the GO showed relatively faint if without any modification, ascribed to that the material lacks strong binding sites towards heavy metal ions(Liu et al. 2019a). Thus, GO as a platform play a crucial role in signal amplification, which allows more PEI and Ab_2 to be labeled.

3.3. Characterization of the Electrochemical Immunosensor

It has been confirmed that electrochemical impedance spectroscopy (EIS) is a

convenient method for estimating the electrochemical property of electrodes at the process of electrode modification(Ye et al. 2019). Impedance spectroscopy involves a linear part (representing a diffusion-limited process) and a semi-circular part (representing an electron transfer-limited process) in which the electron transfer resistance (Ret) is expressed according to the diameter of the semicircle. The EIS value of the electrode surface modification measurement was performed in PBS that contained 5 mM $Fe(CN)_6^{3-/4-}$, and the changes in the Ret value at different electrode modification steps are shown in **Fig. 4**.

The bare electrodes had a small Ret value (curve a), and after exposed to MWCNTs, the semicircle domain significantly shrank, suggesting that the modified electrodes had remarkable electroconductivity (curve b). When the modified-electrodes were decorated with Cu-TCPP(Fe), the semicircle diameter evidently increased (curve c), probably due to the fact that the electrode surface was covered by MOFs, thereby blocking electron transport. After respectively incubated with antigens (curve d), BSA (curve e) and antibodies (curve f) on the electrodes, the value of Ret continued to increase because of presences of the no-electroactive biomaterials, which hindered the electron transfer of $Fe(CN)_6^{3-/4-}$, increasing the distance between the electrode surface and $Fe(CN)_6^{3-/4-}$. When PEI-GO@Ab_2 was modified on the electrode surface, the Ret value dramatically decreased (curve g), meaning that the exposed area of the electrodes and charge transfer capability in the $Fe(CN)_6^{3-/4-}$ solution had obviously improved. The above investigation provided evidence that the immunosensor was successfully fabricated and could be used for target analysis.

3.4. Feasibility of the Detection Methods

Considering that the peroxidase property of Cu-TCPP(Fe) and destroying it using PEI are the two key factors for this immunoassay, they were estimated through a series of investigations. To characterize the electrocatalytic performance of the MOF nanosheets, cyclic voltammetry (CV) was used under different modified electrodes. **Fig. 5** illustrates CVs at a scan rate 100 mV/s and scanning potential from -0.7 V to 0.7 V of bare GCE, bare GCE-modified MWCNTs and bare GCE-modified Cu-TCPP(Fe)/MWCNTs in PBS buffer with/without 10 mM H_2O_2. When H_2O_2 was

present in the reaction system, it was observed that there was a markedly reduced peak current of -0.55 V using Cu-TCPP(Fe)/MWCNTs/GCE (f) in comparison with the bare electrode (e) and MWCNTs/GCE (d), suggesting that Cu-MOFs have excellent peroxidase properties. Compared with the above results, when the reaction solution was only PBS buffer, almost no reduction peak was observed in Cu-TCPP(Fe)/MWCNTs/ GCE(c) due to the absence of H_2O_2 in the detection system. Besides, there are no remarkable change for bare electrode (a) and MWCNTs/GCE (b) when H_2O_2 was introduced into the working buffer, confirming that Cu-TCPP(Fe) was stable enough as nanozyme when being used at the process of sample measurement.

Meanwhile, the dynamic-light-scattering (DLS) measurements indicated that the size of the 2D MOFs decreased after the addition of PEI (illustrated in **Fig. 6A**) probably due to the fact that PEI absorbed the connecting Cu^{2+} metal node of the Cu-MOF nanosheets.

In addition, **Fig. S3** shows that the solution containing Cu-TCPP(Fe) changed from dark brown opaque to brownish yellow transparent after the addition of PEI, indicating that the structure of the MOFs nanosheet has been collapsed. Moreover, amperometric measurements of the immunosensor with different coating layers were employed to estimate the effect of the structure on the electrocatalytic performance of MOFs. As illustrated in **Fig. 6B**, the electrochemical signal response was absent due to the bare GCE (a) does not have the ability to catalyze H_2O_2. Besides, Cu-MOFs /GCE (b) exhibited a marked electrochemical signal in the presence of 10 mM H_2O_2, indicating that Cu-TCPP(Fe) showed excellent electrocatalytic performance for H_2O_2. However, the signal of Cu-MOFs / MWCNTs /GCE (c) was dramatically increase, illustrating that the capacity of electron transfer has been significantly improved by MWCNTs modification. As displayed in **Fig. 6C**, almost no signal was observed when the electrode was decorated with PEI-GO@Ab_2/Ab_1/BSA/Ag/Cu-TCPP(Fe)/MWCNTs/GCE. Although the signal response of GO@Ab_2/Ab_1/BSA/Ag/Cu-TCPP(Fe)/MWCNTs/GCE was decreased, probably due to the fact that GO has a certain functional group to adsorb copper ions

of Cu-TCPP(Fe) and the degree of signal decrease was hardly affect the sensitivity of this work. Thus, these investigations revealed that the structure of Cu-TCPP(Fe) played a decisive role in its electrocatalytic properties.

3.5. Optimization of the Immunosensor

Since some parameters potentially influence the performance of the sensor, they were tested in detail, including reaction time, concentration of antigen/ antibody, Cu-TCPP(Fe) and PEI-GO@Ab_2, which were recorded using amperometric measurements.

As shown in **Fig. 7A and 7B**, the maximum signal was obtained when the antigen and antibody were diluted 8000 and 16,000 times (dilution factor), respectively. In addition, the current response increased when the concentration of 2D MOFs increased from 2 mg/mL to 6 mg/mL, at which point it reached at its peak value. Consequently, 6 mg/mL was considered to be the optimal concentration of Cu-TCPP(Fe) for the detection system (**Fig. 7D**). As shown in **Fig. 7E**, a gradual decrease in the signal was observed at a dilution factor of 1-4 for PEI-GO@Ab_2, and then, the current response increased when the dilution factor exceeded 4; hence, the optimal dilution factor was selected to be 4. At the same time, the most suitable absorption time of Cu^{2+} was 40 min (**Fig. 7F**), and the recognition time between antigen and antibody was 40 min (**Fig. 7C**).

Under the above optimized conditions, the standard curve (**Fig. 8B**) was established after measurement of a serial concentration of SMM (**Fig. 8A**). Good performance was obtained, with a low limit of detection (LOD= $3S_B/m$ = 0.395 ng/mL, where m is the slope of the corresponding calibration curve and S_B is the standard deviation of the blank)(Wang et al. 2014), wide range (1.186- 28.051 ng/mL, IC_{20}-IC_{80})(Fraga et al. 2012), and obvious advantages over other methods (**Table S2**).

3.6. Verification of Accuracy, Stability and Sample Analysis

The accuracy and precision of the established sensor were estimated using a spike-recovery measurement based on water samples from various sources (pure water, pond water, tap water, river water) fortified with a variety of concentrations of SMM**. Table 1** shows that the recoveries of the SAs were in the range of 64-118%

with the intra-assay coefficient of variation (CV) ranging from 2.16% to 7.27%, meaning that the method had good accuracy and could be used for real environmental sample analysis. Besides, the stability of immunosensors was investigated (**Fig. S5**). There are five immunosensors were stored at 4 °C, and assessed every 3 days. The current response retained 83.67% of its initial current after 15 days, indicating that the immunosensors had acceptable stability. The proposed method was applied to investigate the concentration of SAs in real water samples from the Zhenjiang area, Jiangsu Province, China, which was verified by ELISA. As shown in **Table 2**, the results were highly consistent with those from the traditional ELISA method. Meanwhile, compared with ELISA, the proposed immunosensor showed an obvious advantage in sensitivity.

4. Conclusions

In summary, an electrochemical immunosensor was fabricated for ultrasensitive detection of SAs from environmental waters based on the 2D Cu-TCPP(Fe) with peroxidase properties with catalytic H_2O_2 as the signal source. The established method showed good accuracy and reproducibility (recoveries, 64-118%; CV, 2.16-7.27%) with a low LOD of 0.395 ng/mL, which was approximately 4 times lower than that using traditional ELISA with the same antibody (**Fig. S1**). These results suggest that the method has great potential for target analysis. Meanwhile, the present study also provided a novel strategy for designing immunosensors for the determination of other substances with different antibodies.

Acknowledgements

The present work was supported by the National Natural Science Foundation of China (Grants 21577051, 21876067, and 41601552), the Jiangsu Collaborative Innovation Center of Technology and Material of Water Treatment, and the Priority Academic Program Development of Jiangsu Higher Education Institutions (PAPD).

References

Chen, J., Shu, Y., Li, H., Xu, Q., Hu, X., 2018. Nickel metal-organic framework 2D nanosheets with enhanced peroxidase nanozyme activity for colorimetric detection of H2O2. Talanta 189, 254-261.

Cheng, H., Liu, Y., Hu, Y., Ding, Y., Lin, S., Cao, W., Wang, Q., Wu, J., Muhammad, F., Zhao, X., Zhao, D., Li, Z., Xing, H., Wei, H., 2017. Monitoring of Heparin Activity in Live Rats Using Metal-Organic Framework Nanosheets as Peroxidase Mimics. Analytical chemistry 89(21), 11552-11559.

Conzuelo, F., Campuzano, S., Gamella, M., Pinacho, D.G., Reviejo, A.J., Marco, M.P., Pingarrón, J.M., 2013. Integrated disposable electrochemical immunosensors for the simultaneous determination of sulfonamide and tetracycline antibiotics residues in milk. Biosensors and Bioelectronics 50, 100-105.

Conzuelo, F., Gamella, M., Campuzano, S., G. Pinacho, D., Reviejo, A.J., Marco, M.P., Pingarrón, J.M., 2012. Disposable and integrated amperometric immunosensor for direct determination of sulfonamide antibiotics in milk. Biosensors and Bioelectronics 36(1), 81-88.

Dinh, Q., Moreau-Guigon, E., Labadie, P., Alliot, F., Teil, M.-J., Blanchard, M., Eurin, J., Chevreuil, M., 2017. Fate of antibiotics from hospital and domestic sources in a sewage network. Science of The Total Environment 575, 758-766.

Dong, H., Fan, Y., Zhang, W., Gu, N., Zhang, Y., 2019. Catalytic Mechanisms of Nanozymes and Their Applications in Biomedicine. Bioconjugate chemistry.

Du, J., Zhao, H., Liu, S., Xie, H., Wang, Y., Chen, J., 2017. Antibiotics in the coastal

water of the South Yellow Sea in China: Occurrence, distribution and ecological risks. Science of the Total Environment 595, 521-527.

Fraga, M., Vilarino, N., Louzao, M.C., Campbell, K., Elliott, C.T., Kawatsu, K., Vieytes, M.R., Botana, L.M., 2012. Detection of paralytic shellfish toxins by a solid-phase inhibition immunoassay using a microsphere-flow cytometry system. Analytical chemistry 84(10), 4350-4356.

Gao, L., Jie, Z., Leng, N., Zhang, J., Yu, Z., Ning, G., Wang, T., Jing, F., Yang, D., Perrett, S., 2007. Intrinsic peroxidase-like activity of ferromagnetic nanoparticles. Nature Nanotechnology 2(9), 577-583.

Hernández-Mesa, M., Moreno-González, D., Lara, F.J., García-Campaña, A.M., 2019. Electrophoresis | Capillary Electrophoresis: Food Chemistry Applications. In: Worsfold, P., Poole, C., Townshend, A., Miró, M. (Eds.), Encyclopedia of Analytical Science (Third Edition), pp. 358-366. Academic Press, Oxford.

Huang, A., Bo, F., 2018. Facile synthesis of PEI-GO@ZIF-8 hybrid material for CO 2 capture. International Journal of Hydrogen Energy 43(4), S0360319917347080.

Huang, Y., Zhao, M., Han, S., Lai, Z., Yang, J., Tan, C., Ma, Q., Lu, Q., Chen, J., Zhang, X., Zhang, Z., Li, B., Chen, B., Zong, Y., Zhang, H., 2017. Growth of Au Nanoparticles on 2D Metalloporphyrinic Metal-Organic Framework Nanosheets Used as Biomimetic Catalysts for Cascade Reactions. Advanced materials 29(32).

Jia, W., Shi, L., Chu, X., 2018. Untargeted screening of sulfonamides and their metabolites in salmon using liquid chromatography coupled to quadrupole Orbitrap mass spectrometry. Food Chemistry 239, 427-433.

Jing, X., Mi, H.-Y., Napiwocki, B.N., Peng, X.-F., Turng, L.-S., 2017. Mussel-inspired electroactive chitosan/graphene oxide composite hydrogel with rapid self-healing and recovery behavior for tissue engineering. Carbon 125, 557-570.

Kim, H., Hong, Y., Park, J.-e., Sharma, V.K., Cho, S.-i., 2013. Sulfonamides and tetracyclines in livestock wastewater. Chemosphere 91(7), 888-894.

Liu, T.Z., Hu, R., Zhang, X., Zhang, K.L., Liu, Y., Zhang, X.B., Bai, R.Y., Li, D., Yang, Y.H., 2016. Metal-Organic Framework Nanomaterials as Novel Signal Probes for Electron Transfer Mediated Ultrasensitive Electrochemical Immunoassay. Analytical chemistry 88(24), 12516-12523.

Liu, X., Ma, R., Ma, Y., Yang, Y., Zhuang, L., Zhang, S., Jehan, R., Chen, J., Wang, X., 2019a. Graphene oxide-based materials for efficient removal of heavy metal ions from aqueous solution: A review. Environmental Pollution 252.

Liu, X., Yan, Z., Zhang, Y., Liu, Z., Sun, Y., Ren, J., Qu, X., 2019b. Two-Dimensional Metal-Organic Framework/Enzyme Hybrid Nanocatalyst as a Benign and Self-Activated Cascade Reagent for in Vivo Wound Healing. ACS Nano.

Loos, R., Tavazzi, S., Mariani, G., Suurkuusk, G., Paracchini, B., Umlauf, G., 2017. Analysis of emerging organic contaminants in water, fish and suspended particulate matter (SPM) in the Joint Danube Survey using solid-phase extraction followed by UHPLC-MS-MS and GC–MS analysis. Science of The Total Environment 607-608, 1201-1212.

Lu, Z., Na, G., Gao, H., Wang, L., Bao, C., Yao, Z., 2015. Fate of sulfonamide resistance genes in estuary environment and effect of anthropogenic activities.

374 Science of The Total Environment 527-528, 429-438.

375 Luo, Y., Mao, D.Q., Rysz, M., Zhou, Q.X., Zhang, H.J., Xu, L., Alvarez, P.J.J., 2010.
376 Trends in antibiotic resistance genes occurrence in the Haihe River, China.
377 Environmental Science & Technology 44(19), 7220.

378 Ma, M., Wen, K., Beier, R.C., Eremin, S.A., Li, C., Zhang, S., Shen, J., Wang, Z.,
379 2016. Chemiluminescence Resonance Energy Transfer Competitive Immunoassay
380 Employing Hapten-Functionalized Quantum Dots for the Detection of Sulfamethazine.
381 ACS Applied Materials & Interfaces 8(28), 17745-17750.

382 Managaki, S., Murata, A., Takada, H., Tuyen, B.C., Chiem, N.H., 2007. Distribution
383 of Macrolides, Sulfonamides, and Trimethoprim in Tropical Waters: Ubiquitous
384 Occurrence of Veterinary Antibiotics in the Mekong Delta. Environmental Science &
385 Technology 41(23), 8004-8010.

386 Nebot, C., Regal, P., Miranda, J.M., Fente, C., Cepeda, A., 2013. Rapid method for
387 quantification of nine sulfonamides in bovine milk using HPLC/MS/MS and without
388 using SPE. Food Chemistry 141(3), 2294-2299.

389 Qin, L., Wang, X., Liu, Y., Wei, H., 2018a. 2D-Metal-Organic-Framework-Nanozyme
390 Sensor Arrays for Probing Phosphates and Their Enzymatic Hydrolysis. Analytical
391 chemistry 90(16), 9983-9989.

392 Qin, L., Wang, X., Liu, Y., Wei, H., 2018b. 2D-Metal–Organic-Framework-Nanozyme
393 Sensor Arrays for Probing Phosphates and Their Enzymatic Hydrolysis. Analytical
394 chemistry 90(16), 9983-9989.

395 Shan, D., Zhu, M., Xue, H., Cosnier, S., 2007. Development of amperometric

biosensor for glucose based on a novel attractive enzyme immobilization matrix: calcium carbonate nanoparticles. Biosensors & bioelectronics 22(8), 1612-1617.

Shoeib, M., Harner, T., Ikonomou, M., Kannan, K., 2004. Indoor and outdoor air concentrations and phase partitioning of perfluoroalkyl sulfonamides and polybrominated diphenyl ethers. Environmental Science & Technology 38(5), 1313-1320.

Shuo, Z., Hao-Tian, W., Ke, L.I., Jing, Z., Xia-Yan, W., Guang-Sheng, G.U.O., 2018. Fast Determination of Residual Sulfonamides in Milk by In-Tube Solid-Phase Microextraction Coupled with Capillary Electrophoresis-Laser Induced Fluorescence. Chinese Journal of Analytical Chemistry 46(3), e1810-e1816.

Walper, S.A., Lasarte Aragones, G., Sapsford, K.E., Brown, C.W., 3rd, Rowland, C.E., Breger, J.C., Medintz, I.L., 2018. Detecting Biothreat Agents: From Current Diagnostics to Developing Sensor Technologies. ACS sensors 3(10), 1894-2024.

Wang, H., Bai, L., Chai, Y., Yuan, R., 2014. Synthesis of multi-fullerenes encapsulated palladium nanocage, and its application in electrochemiluminescence immunosensors for the detection of Streptococcus suis Serotype 2. Small 10(9), 1857-1865.

Won, S.Y., Lee, C.H., Chang, H.S., Kim, S.O., Lee, S.H., Kim, D.S., 2011. Monitoring of 14 sulfonamide antibiotic residues in marine products using HPLC-PDA and LC-MS/MS. Food Control 22(7), 1101-1107.

Ye, J., Zhu, L., Yan, M., Zhu, Q., Lu, Q., Huang, J., Cui, H., Yang, X., 2019. Dual-Wavelength Ratiometric Electrochemiluminescence Immunosensor for Cardiac

418 Troponin I Detection. Analytical chemistry 91(2), 1524-1531.

419 Zhang, N., Zang, G.L., Shi, C., Yu, H.Q., Sheng, G.P., 2016. A novel adsorbent
420 TEMPO-mediated oxidized cellulose nanofibrils modified with PEI: Preparation,
421 characterization, and application for Cu(II) removal. J Hazard Mater 316, 11-18.

422 Zhang, X., Li, G., Wu, D., Li, X., Hu, N., Chen, J., Chen, G., Wu, Y., 2019. Recent
423 progress in the design fabrication of metal-organic frameworks-based nanozymes and
424 their applications to sensing and cancer therapy. Biosensors & bioelectronics 137,
425 178-198.

426 Zhou, Y., Liu, B., Yang, R., Liu, J., 2017. Filling in the Gaps between Nanozymes and
427 Enzymes: Challenges and Opportunities. Bioconjugate chemistry 28(12), 2903-2909.

428 Zhu, X., Ji, H., Yi, J., Yang, J., She, X., Ding, P., Li, L., Deng, J., Qian, J., Xu, H., Li,
429 H., 2018. A Specifically Exposed Cobalt Oxide/Carbon Nitride 2D Heterostructure for
430 Carbon Dioxide Photoreduction. Industrial & Engineering Chemistry Research 57(51),
431 17394-17400.

432 Zhu, X., Yang, J., She, X., Song, Y., Qian, J., Wang, Y., Xu, H., Li, H., Yan, Q., 2019.
433 Rapid synthesis of ultrathin 2D materials through liquid-nitrogen and microwave
434 treatments. Journal of Materials Chemistry A 7(10), 5209-5213.

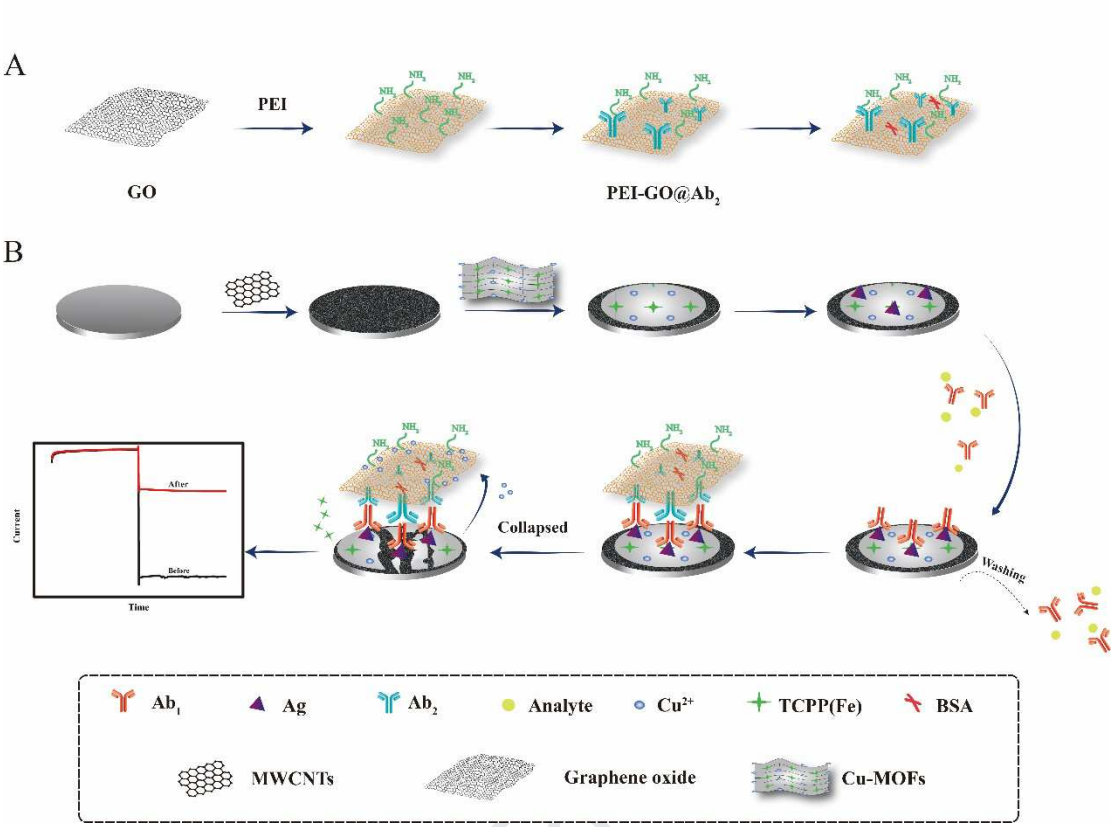

435

436 **Scheme 1.** Schematic illustration of the electrochemical immunosensor for the

437 detection of Sulfonamides.

438

Figure captions

Fig. 1. TEM image of Cu-TCPP(Fe) (A); SEM image of Cu-TCPP(Fe) (B); EDS of Cu-TCPP(Fe) (C).

Fig. 2. TEM image of GO (A), PEI-GO (B); SEM image of GO (C), PEI-GO (D).

Fig. 3. The FT-IR spectra of GO (a), PEI-GO (b).

Fig. 4. EIS characterization of electrodes at various steps of modification in 5 mM [$Fe(CN)_6]^{3-/4-}$] solution: bare GCE(a), MWCNTs/GCE(b), Cu-TCPP(Fe)/MWCNTs/GCE(c), Ag/Cu-TCPP(Fe)/MWCNTs/GCE(d), BSA/Ag/Cu-TCPP(Fe)/MWCNTs/GCE(e), Ab_1/BSA/Ag/Cu-TCPP(Fe)/MWCNTs/GCE(f), PEI-GO@Ab_2/Ab_1/BSA/Ag/Cu-TCPP(Fe)/MWCNTs/GCE(g).

Fig. 5. The CV of the immunosensor with different modified electrodes in blank (a: bare GCE, b: MWCNTs/GCE, c: Cu-TCPP(Fe)/MWCNTs/GCE) and containing 10 mM H_2O_2(d: bare GCE, e: MWCNTs/GCE, f: Cu-TCPP(Fe)/MWCNTs/GCE).

Fig. 6. DLS characterization of Cu-TCPP(Fe) before (black) and after (red) with PEI (A); The i-t curve of the immunosensor with different modified electrodes in PBS containing 10 mM H_2O_2: (B) bare GCE(a), Cu-TCPP(Fe)/GCE(b) and Cu-TCPP(Fe)/MWCNTs/GCE(c); (C) Ab_1/BSA/Ag/Cu-TCPP(Fe)/MWCNTs/GCE(a), GO@Ab_2/Ab_1/BSA/Ag/Cu-TCPP(Fe)/MWCNTs/GCE(b) and PEI-GO@Ab_2/Ab_1/BSA/Ag/Cu-TCPP(Fe)/MWCNTs/GCE(c).

Fig. 7. Effect of the dilution of antibody (A) and antigen (B), the recognition time of antibody and antigen (C) the concentration of Cu-TCPP(Fe) (D), the dilution of PEI-GO@Ab_2 (E) and the time of Cu^{2+} absorption (F). Error bars = RSD (n=3).

Fig. 8. The amperometric method measurements of the fabricated immunosensor after incubating with 0-81 ng/mL SMM. (a) 0, (b) 0.1, (c) 0.3, (d) 0.9, (e) 3, (f)9, (g)27, (h) 81 ng/mL SMM in PBS (pH 7) containing 10 mM H_2O_2 (A); The standard curves of the indirect competitive electrochemical immunosensor for SMM under the optimized conditions (B). Error bars = RSD (n=3).

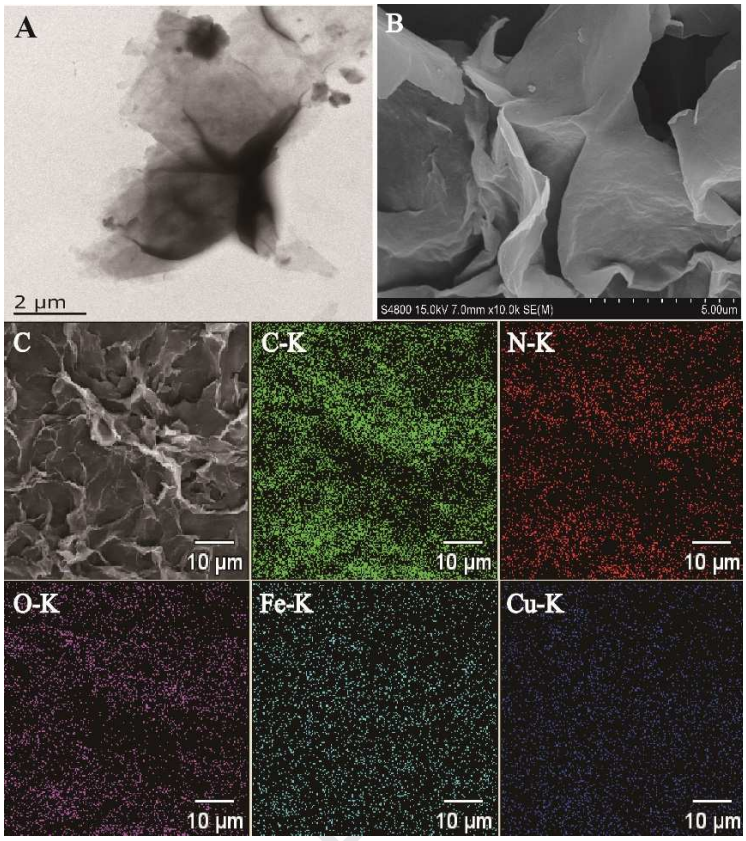

468

469 **Fig. 1.** TEM image of Cu-TCPP(Fe) (A); SEM image of Cu-TCPP(Fe) (B); EDS of

470 Cu-TCPP(Fe) (C).

471

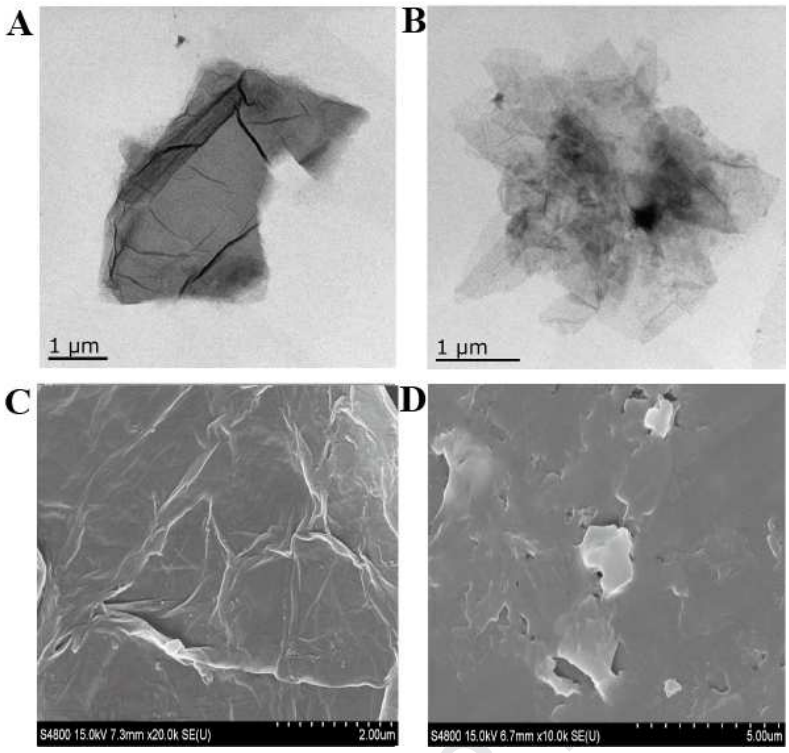

Fig. 2. TEM image of GO (A), PEI-GO (B); SEM image of GO (C), PEI-GO (D).

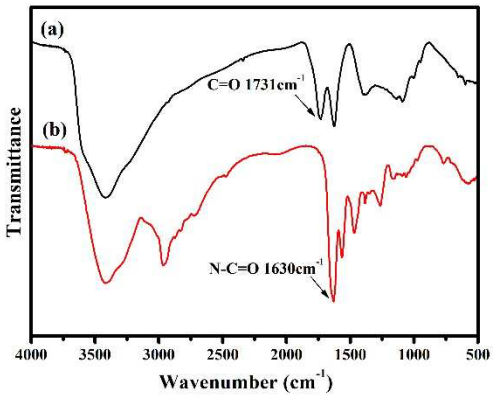

475

476 **Fig. 3.** The FT-IR spectra of GO (a), PEI-GO (b).

477

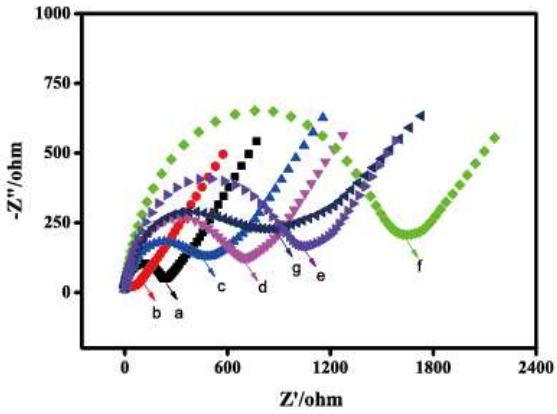

478

479 **Fig. 4.** EIS characterization of electrodes at various steps of modification in 5 mM [Fe
480 $(CN)_6]^{3-/4-}$] solution: bare GCE(a), MWCNTs/GCE(b),
481 Cu-TCPP(Fe)/MWCNTs/GCE(c), Ag/Cu-TCPP(Fe)/MWCNTs/GCE(d),
482 BSA/Ag/Cu-TCPP(Fe)/MWCNTs/GCE(e),
483 Ab_1/BSA/Ag/Cu-TCPP(Fe)/MWCNTs/GCE(f),
484 PEI-GO@Ab_2/Ab_1/BSA/Ag/Cu-TCPP(Fe)/MWCNTs/GCE(g).

485

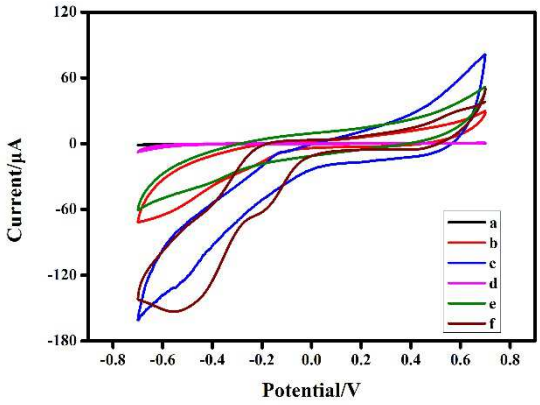

Fig. 5. The CV of the immunosensor with different modified electrodes in blank (a: bare GCE, b: MWCNTs/GCE, c: Cu-TCPP(Fe)/MWCNTs/GCE) and containing 10 mM H_2O_2(d: bare GCE, e: MWCNTs/GCE, f: Cu-TCPP(Fe)/MWCNTs/GCE).

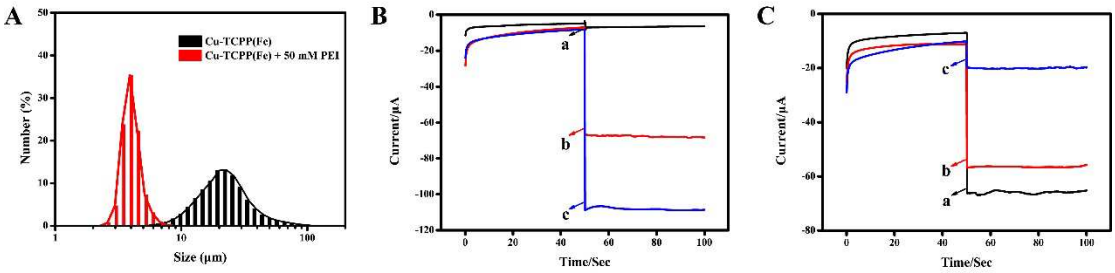

Fig. 6. DLS characterization of Cu-TCPP(Fe) before (black) and after (red) with PEI (A); The i-t curve of the immunosensor with different modified electrodes in PBS containing 10 mM H_2O_2: (B) bare GCE(a), Cu-TCPP(Fe)/GCE(b) and Cu-TCPP(Fe)/MWCNTs/GCE(c); (C) Ab_1/BSA/Ag/Cu-TCPP(Fe)/MWCNTs/GCE(a), GO@Ab_2/Ab_1/BSA/Ag/Cu-TCPP(Fe)/MWCNTs/GCE(b) and PEI-GO@Ab_2/Ab_1/BSA/Ag/Cu-TCPP(Fe)/MWCNTs/GCE(c).

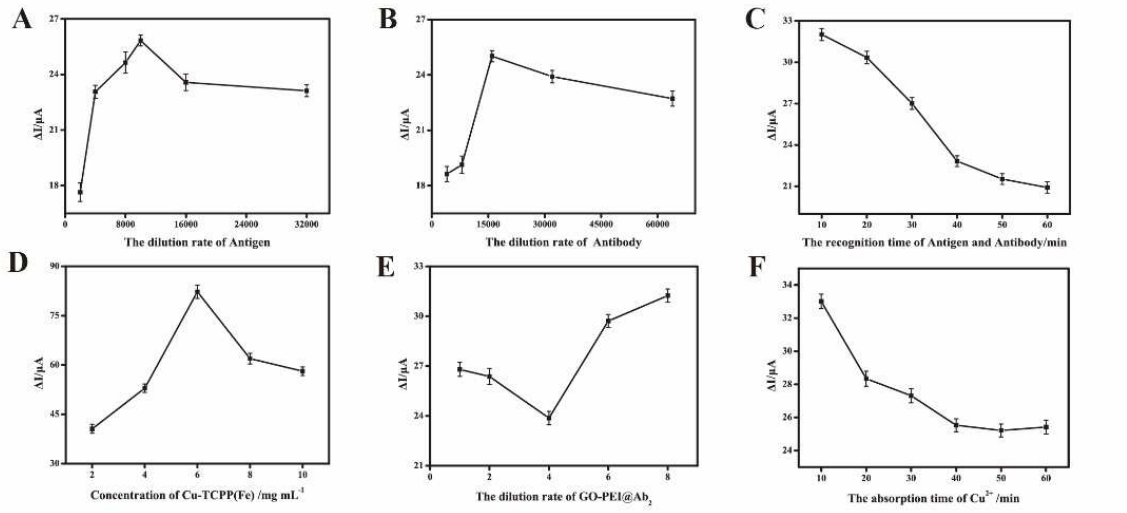

500

501 **Fig. 7.** Effect of the dilution of antibody (A) and antigen (B), the recognition time of
502 antibody and antigen (C) the concentration of Cu-TCPP(Fe) (D), the dilution of
503 PEI-GO@Ab_2 (E) and the time of Cu^{2+} absorption (F). Error bars = RSD (n=3).

504

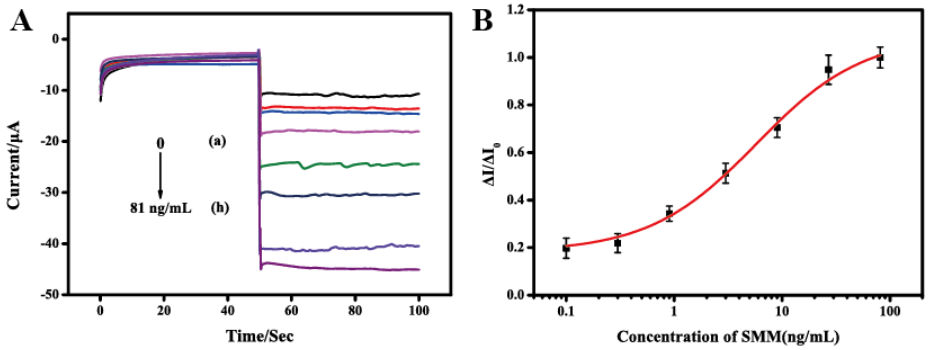

505

506 **Fig. 8.** The amperometric method measurements of the fabricated immunosensor after
507 incubating with 0-81 ng/mL SMM. (a) 0, (b) 0.1, (c) 0.3, (d) 0.9, (e) 3, (f)9, (g)27, (h)
508 81 ng/mL SMM in PBS (pH 7) containing 10 mM H_2O_2 (A); The standard curves
509 (y=1.09072-0.9091/(1+ (x/5.76723) ^0.87639), correlation coefficient 0.993) of the
510 indirect competitive electrochemical immunosensor for SMM under the optimized
511 conditions (B). Error bars = RSD (n=3).

512

Table captions

Table 1. Analysis of SA-spiked using our established method (n=3).

Table 2. The comparison for SAs detection using our established method and the conventional ELISA (n=3).

518 **Table 1.** Analysis of SA-spiked using our established method (n=3).

Samples	Background (ng/mL)	Added (ng/mL)	Found (ng/mL)	Recovery (%)	CV[a] (%)
Pure water	ND[b]	1.5	1.77	118	2.38
		5	3.20	82	3.21
		25	27.25	109	2.16
Pond water	5.41	1.5	7.67	111	2.64
		5	9.11	74	5.58
		25	27.16	87	2.94
Tap water	ND	1.5	1.61	107	3.54
		5	4.55	91	7.27
		25	22.00	88	2.93
River water	3.20	1.5	5.2	110	2.87
		5	5.25	64	3.02
		25	21.75	77	3.42

519 [a] CV, intra-assay coefficient of variation obtained from 3 determinations performed in the same
520 polystyrene microtiter plate.
521 [b] ND, not detected.
522

523 **Table 2.** The comparison for SAs detection using our established method and the
524 conventional ELISA (n=3).

Samples	ELISA (ng/mL)	Our method (ng/mL)	CV (%)
S1	8.29	6.13	2.57
S2	ND	2.92	4.65
S3	27.83	25.83	3.76
S4	ND	2.31	3.21
S5	ND	ND	/
S6	4.92	3.24	4.15
S7	13.52	10.87	3.68
S8	ND	2.76	4.26
S9	16.95	14.53	4.62
S10	3.92	2.01	3.85
S11	7.31	5.27	4.93
S12	9.52	6.93	2.86
S13	ND	2.42	3.61
S14	5.87	3.15	4.82
S15	ND	ND	/

525 [a] CV, intra-assay coefficient of variation obtained from 3 determinations performed in the same
526 polystyrene microtiter plate.
527 [b] ND, not detected.

Highlights

1. A novel competitive electrochemical immunosensor strategy was fabricated for determination of SAs with a low LOD of 0.395 ng/mL;
2. The good performance was benefited from a nanozyme (2D Cu-TCPP(Fe)) used, which was directly modified on the electrodes, preventing the decrease in catalytic efficiency during nanozyme labeling;
3. The signal amplification was ascribed to the collapsed structure of 2D Cu-TCPP(Fe) by PEI-GO, resulting in remarkably decreased catalytic ability;
4. The immunosensor showed satisfactory accuracy (recoveries, 64-118%; CV, 2.16% - 7.27%) and a good detection range (1.186-28.051 ng/mL).

credit author statement

Jiaxuan Xiao and Xialin Hu designed experiments; Jiaxuan Xiao, Eric Gyimah and Salome Yakubu carried out experiments; Jiaxuan Xiao analyzed experimental results; Jiaxuan Xiao analyzed sequencing data and developed analysis tools; Kun Wang, Yanmin Zou and Xialin Hu assisted with illumina sequencing; Jiaxuan Xiao, Xialin Hu and Zhen Zhang wrote the manuscript.

Declaration of interests

☒ The authors declare that they have no known competing financial interests or personal relationships that could have appeared to influence the work reported in this paper.

☐The authors declare the following financial interests/personal relationships which may be considered as potential competing interests: